Color Scene Analysis in the 1976 CIE (L*a*b*) Uniform Color Space

Mehmet Celenk
Department of Electrical and Computer Engineering, Ohio University, Athens, Ohio

Abstract

This paper describes a scene analysis method that detects object surfaces using color information. The proposed method operates in the 1976 CIE (L*,a*,b*) uniform color space and utilizes the Munsell color order system as a reference. The textured scene or object surfaces are identified by Julesz's conjecture. The technique presented in this paper was applied to several low contrast 580×700 color images of a city skyline taken in winter with 8 bits/pixel R, G, B specification.

1. Introduction

Object surface detection is the critical first step in image information extraction for computer vision systems. This process determines the structural characteristics of objects' surfaces using detailed image domain properties. Achieving an adequate scene description depends mainly on devising techniques to detect uniformity among the feature values of the picture points, and then isolating the areas of the picture exhibiting these uniformities.[2,3] Clustering has been extensively used for analyzing and segmenting the color pictures.[4-10, 33] However, color clustering is a computationally expensive process[11] since the feature space is three dimensional. One solution to this problem is to project the feature space onto 2-D planes as described in Refs. [6,7,8]. Another alternative is to develop efficient methods of storing and processing the 3-D color data as reported in Refs. [9,10]. A more effective method as described here is to project the color space onto the selected coordinate axes repeatedly until the image clusters are enclosed in some specified volume elements. From each projection of the space, we determine one particular surface of the decision elements. This estimates the clusters' distributions in the 3-D color space without imposing any constraints on their forms. The goal here is to reduce the computational cost involved in maintaining many derived images and their respective histograms and in forming 3-D decision surfaces. The estimated color clusters are then projected onto the line of Fisher discriminant[23] for 1-D thresholding using the information obtained from the 3-D feature space. This permits utilization of all the property values of clusters for segmentation, and inherently recognizes their respective cross correlation. This way, the region acceptance is not limited to the information available from one color component. An additional feature set is needed to give rise to such modes in the respective histograms in the absence of image clusters. For this purpose, a feature extraction algorithm[27] is devised based on Julesz's conjecture by integrating the spatial and spectral information of image points in the local image areas. This integration provides a better clustering in the measurement space than the sensory data alone as demonstrated in the paper.

2. Background

A color image is given by the R (red), G (green), and B (blue) tristimuli at every pixel. Several features[12-15 ,9, 32] can be calculated from the tristimuli for different purposes. For color clustering, it is desirable that the selected color features define a uniform space possessing uniform.[16, 17, 32] It has been shown in Ref. [15] that the (L*, a*, b*) uniform color coordinate system developed by the CIE[18] in 1976 gives better results than the other spaces in segmenting the color pictures. This system is obtained from the (R, G, B) – primary system by converting the (R, G, B) values into the (X, Y, Z) – nonphysical primary system[21] and applying a cube-root transformation:

$$X = 2.7690R + 1.7518G + 1.1300B \quad (1.1)$$
$$Y = 1.0000R + 4.5907G + 0.0601B \quad (1.2)$$
$$Z = 0.0000R + 0.0565G + 5.5943B \quad (1.3)$$

$$L^* = 116[Y/Y_o]^{1/3} - 16 \quad (2.1)$$
$$a^* = 500[(X/X_o)^{1/3} - (Y/Y_o)^{1/3}] \quad (2.2)$$
$$b^* = 200[(Y/Y_o)^{1/3} - (Z/Z_o)^{1/3}] \quad (2.3)$$

where X_o, Y_o, and Z_o are the (X,Y,Z) values of the reference white (255 for 8 bit image data representation) and satisfy the condition that $X/X_o > 0.01$, $Y/Y_o > 0.01$, $Z/Z_o > 0.01$. Fig. 1 shows the organization of (L*, a*, b*) cube-root system. The cylindrical coordinates (L*: lightness, H°: hue, C*: chroma)[22] of this space resemble the empirical Munsell color order system[19] and concur almost exactly with the accepted physiological model of color vision.[20] They are given by (see also Fig. 1)

$$L^* = L^* \quad (3.1)$$
$$H^o = \tan^{-1}(b^*/a^*) \quad (3.2)$$
$$C^* = (a^{*2}+b^{*2})^{1/2} \quad (3.3)$$

In Fig. 2, organization of the constant chromaticity network of the Munsell system are shown for twenty hues (varying from 5R to 10RP) at eight chroma values (increasing from /2 to /16) in the (a*, b*)-plane for the Munsell value of 5/. Here this network is explored for estimating the 3-D color distributions of image clusters. For this purpose, the radial hue and concentric chroma

loci are approximated by radial lines and concentric circles in the least square sense as shown in Fig. 2. They are used to estimate the clusters' distributions in some circular-cylindrical volume elements in the (L*, a*, b*) space. Fig. 3 shows such a decision element which is bounded by two lightness planes (L^*_1 and L^*_2), two hue planes (H^o_1 and H^o_2), and two chroma cylinders (C^*_1 and C^*_2). This gives the nonparametric estimates of the clusters' distributions in the 3-D color space. This is similar to the process described in Ref. [8], which relies on the use of elliptical and parabolic decision surfaces to enclose image clusters in the X-Y, X-I, and Y-I plane projections of the (X,Y,I) normalized color space. However, use of the chromaticity network results in simpler decision surfaces than those obtained in Ref. [8]. Furthermore, here the cluster detection is performed in the 3-D color space instead of its lower dimensional subspaces as proposed in Ref. [8]. This permits utilization of all the property values of clusters for segmentation, and inherently recognizes their respective cross correlation. This way, the region acceptance is not limited to the information available from one color component.

2. Description of the Method

Consider the 1-D histograms of L^*, H^o, and C^* color coordinates of the test image given in Fig. 5. From these distributions, the best decisive peak (M1) and its largest neighbor (M2) are located in the hue histogram. (For peak acceptance procedure see Refs. [30,31,34].) In the hue scale, the range of M1 (H^o_{M1}) varies from 170° to 284° and the range of M2 (H^o_{M2}) lies from 74° to 170°. These planes describe the hue variation of the most prominent cluster (w_1) and its largest spectral neighbor (w_2) (see Fig. 6).

The space distribution of w_1 is obtained using the 1-D histograms of L* and C* color components of the image pixels whose hue values are in the hue range of the mode M1. These distributions for the test image are given in Fig. 7. Each possesses only one decisive peak. The lightness and chroma ranges (L^*_{M1} and C^*_{M1}) of these peaks are given by $74 < L^* < 94$ and $0 < C^* < 19$. The lightness values 74 and 94 define two constant horizontal lightness planes in the space and the chroma value 19 specifies a constant circular cylinder around the lightness axis. These loci describe the lightness and chroma variation of w_1 as depicted in Figs. 8 and 9. It is clear that the respective loci of the constants (170°, 284°), (74, 94), and (0, 19) represent a circular-cylindrical decision volume V_1 in the (L*, a*, b*) space (Fig. 10) as the estimated color distribution of w_1.

The process described above is then repeated for estimating the color distribution of w_2. Fig. 11 shows the 1-D histograms of L* and C* color components of the image points whose hue values lie within the hue range of w_2. From these two distributions, the lightness and chroma ranges (L^*_{M2} and C^*_{M2}) of w_2 are given by $79 < L^* < 96$ and $0 < C^* < 27$. The lightness values 79 and 96 define two horizontal planes in the space and the chroma value 27 describes an eccentric cylinder around the achromatic axis. These surfaces are also plotted in Figs. 8 and 9. The respective loci of the constants (74°, 170°), (79, 96), and (0, 27) also characterize a volume element V_2 in the space as the estimated distribution of w_2. This volume is also illustrated in Fig. 10 by showing its position with respect to that of w_1.

It is clear from Fig. 10 that the estimated distributions (V_1 and V_2) of w_1 and w_2 have a significant overlap along the L* axis due to their lightness ranges. In order to minimize the effect of this overlap in region isolation, the most prominent cluster w_1 is separated from its spectral neighbor w_2 using all the information gathered from the 3-D color space. This isolation process is carried out using the Fisher linear discriminant function. A similar study was also made in Refs. [24, 25] for pixel classification and target detection. Here, this technique is explored for isolating the detected color clusters of natural scenes as a two-at-a-time class separation process as follows: The color vectors of w_1 and w_2 are projected onto the line of Fisher discriminant

$$W = [S_1 + S_2]^{-1}. (M_1 - M_2) \quad (4)$$

so that the projected color points are well clustered and separated for 1-D thresholding (see Fig. 12). Here (S_1, S_2) and (M_1, M_2) are the covariance matrices and the mean vectors of classes 1 and 2, respectively. W defines a direction in the feature space, which is independent of the class distribution functions.

For the detected clusters of the test image, the line of projection is computed as $W = [-0.07407\ 0.32801\ -0.20976]^T$, where T denotes the transpose of the row matrix. The color vectors of the image points, which are the elements of w_1 and w_2 (see Fig. 10), are then projected onto this line using

$$d(C) = W^T. C \quad (5)$$

Here, d is the linear discriminant and C is the color vector of the image pixels belonging to V_1 or V_2.

The 1-D histogram of the projected data points is given in Fig. 13. The projected values of the class mean vectors are also computed as $d_{M1} = 65.775$ and $d_{M2} = 25.295$. Comparing the value of d_{M1} with the valley between the histogram peaks, a threshold is set in this histogram as $d > 42$ to create a binary picture for the image region of w_1. This segment is further refined in the spatial domain using a set of binary smoothing templates.[26] The final result is shown in Fig. 14.a, which corresponds to the sky.

The above detection and isolation algorithms are then applied to the remaining image points which yield the 1-D histograms of Fig. 15. Two peaks in the lightness distribution are selected as the best mode (M_1) and its neighbor (M_2) which lie in the lightness range of $80 < L^* < 100$ and $0 < L^* < 80$. Projecting the image clusters due to these two peaks onto $W = [0.18654\ -0.00102\ 0.01216]^T$ results in a 1-D histogram (Fig. 16) possessing two peaks. By setting a threshold at 14.5 of the histogram variable, a binary picture is created and further refined in the spatial domain using the smoothing templates. The resultant regions, called "11:BLRI" are shown in Fig. 14.b, which correspond to the leftmost building and river.

Since the 1-D histograms (see Fig. 17) of the remaining part of the test image do not exhibit any decisive peak, an additional feature set is needed to give rise to 1-

D clusters in the image histograms. For this, the remaining part of the test image is first partitioned into its atomic regions of maximally 4-connected pixels of the similar color. For this partitioning, every unprocessed pixel is initially assumed to be an atomic region by assigning it a region number. Starting from the first row and first column, the color vector of each unclassified point is compared with that of its left and top neighbors. If a similarity between the pixel in process and any of its specified neighbors in a 3×3 local window is detected, then the region number of that element is modified to that of its similar neighbor. Here the similarity between an image pixel (i, j) and its left or top neighbor (m, n) is defined by

$$| L^*(i,j) - L^*(m,n) | < 10 \quad (6.1)$$

$$| H^o(i,j) - H^o(m,n) | < 10^o \quad (6.2)$$

$$| H^o(i,j) - H^o(m,n) | > 350^o \quad (6.3)$$

$$| C^*(i,j) - C^*(m,n) | < 10 \quad (6.4)$$

The outlined region growing technique is repeated at every unprocessed point of the test image. The total number of atomic regions created for the remaining points of the test picture is 2171.

After this initial partitioning, the algorithm computes the center of gravity of every atomic region a_k using

$$i_k = \sum_i \sum_j |c(i,j)| i \Big/ \sum_i \sum_j |c(i,j)| \quad (7.1)$$

$$j_k = \sum_i \sum_j |c(i,j)| j \Big/ \sum_i \sum_j |c(i,j)| \quad (7.2)$$

where | C(i,j) | is the magnitude of the color vector of a point (i, j) in a_k. A 30×30 local window is then located at the center of the atomic region in process. Within this window, eight fixed directions are defined from the center of that atomic region (see Fig. 18). On each of these directions, similarity between the atomic region in question and its neighbors is tested according to the similarity criteria given by the Eqs. 6.1-4. If the continuity property is observed along these directions, the atomic region of interest is classified as being a part of a uniform region and its feature vector is computed in the corresponding direction(s). If the continuity search fails, then a possible periodic texture structure is sought to classify the atomic region as being a spectral primitive of a texture field and to compute its feature vector in the respective directions. In the absence of continuity and texture patterns, the atomic region is accepted as an isolated one and its feature assignment is made considering all of its touching neighbors.

Once an atomic region is classified as being a part of a visual pattern through the specified directions, then the feature vector f is assigned to that atomic region by averaging the color vectors of the atomic regions in that visual pattern as described below:

$$f = E\{C_k \cup C_l\} \quad (8)$$

Here, C_k and C_l are the color vectors of the atomic region a_k and its neighbors in the determined directions, E is the expected value operator, and U represents the union of color vectors.

The above feature extraction technique yield a feature set f for the remaining points of the test image that provides the 1-D histograms of Fig. 19. Comparing the L* histogram of Fig. 19 with that of Fig. 17, it can be noticed that the L* component of f gives a better clustering property than that of the sensory data. The former histogram possesses two 1-D clusters in contrast to the latter. These decisive 1-D peaks are defined in the lightness scale as $62 < L^* < 100$ and $0 < L^* < 62$.

Projecting the 3-D clusters due to these two peaks onto the line $W = [0.25864\ 0.01177\ 0.02304]^T$ results in the histogram of Fig. 20. By setting a threshold at 17.5, the resultant region, called "11:APM", is obtained as shown in Fig. 14.c. This represents the building at the center of the test image.

The remaining points of the test image are accepted as a uniform region with respect to the extracted feature vector f. After the spatial refinement, the resultant regions, called "11:APS", are obtained as shown in Fig. 14.d. They are the midleft and rightmost buildings in the scene.

4. Experimental Results

The method described here was applied to several low contrast color images of the skyline of Pittsburgh city taken in winter. The spectral contents of the images are limited mainly to the bright colors (usually $C^* < 30$ and $L^* > 60$). The original images are given with the 8 bits/pixel R, G, B specification in 580×700 grid. In order to fit the image data to the computer system (DEC PDP-10) used in the implementation, the pictures were reduced to 193×232 grid by a factor of 3 in each dimension. This reduction significantly affected the spatial resolution of the resultant images. For example, the textured buildings located in the middle of the test image shown in Fig. 4, became almost a wide building block. Although the separation of these two buildings along a straight line is almost impossible by an observer, the algorithm gives a reasonably good segmentation result by locating this straight line between the buildings. Four images were segmented in the computer implementation of the method.[27-29,35,36] Two of these pictures are shown in Figs. 4 and 21. All the visually distinct areas of the test image given in Fig. 4 were successfully extracted as described earlier. Some of the processing results of the other poor resolution image, called picture "9", are presented in Fig. 22.

5. Conclusions

This paper has described a color scene analysis technique in the (L*, a*, b*) cube-root color coordinate system using all the color property values of object surfaces for analysis. The result obtained with this method is also compared with the result produced using a single color component of the (L*, a*, b*) system. For example, we have used the hue component of the peak determined within 170° to 284° range of the distribution of Fig. 5 to obtain the scene area. Boundaries of the resultant region (sky) have severely deformed and many fine grain image segments have resulted along the boundary. The proposed technique however gave reasonably good result by locating the straight line to separate the sky from the buildings in the image.

References

1. E. M. Riseman, et al., Computational techniques in the visual segmentation of static scenes, *CGIP* **6:** 221-276 (1977).
2. K. S. Fu, et al., A survey on image segmentation, *PR* **13:** 3-16 (1981).
3. R. M. Haralick, et al., Image segmentation techniques, *CVGI* **29:** 100- 132 (1985).
4. R. Ohlander, et al., Picture segmentation using a recursive region splitting method, *CGIP* **8:** 313-333 (1978).
5. J. M. Tenenbaum, et al., An interactive facility for scene analysis research, *Tech. Note 87*, AI Center, SRI, CA, 1974.
6. S. A. Underwood, et al., Interactive computer analysis of aerial color infrared photographs, *CGIP* **6:** 1-24 (1977).
7. M. Ali, et al., Automatic interpretation of infrared aerial color photographs of citrus orchards having infestations of insect pests and diseases, *IEEET- GE* **15(3):** 170-179 (1977).
8. M. Ali, et al., Color-based computer analysis of aerial photographs, *CGIP* **9:** 282- 293 (1979).
9. B. J. Schacter, et al., Scene segmentation by cluster detection in color space, *Tech. Rep.-424*, Univ. of Maryland, 1975.
10. A. Sarabi, et al., Segmentation of chromatic images, *PR* **13:** 417-427 1981).
11. R. Gershon, Aspects of perception and computation in color vision, *CVGIP* **32:** 244-277 (1985).
12. T. Kanade, Region segmentation: Signal vs semantics, *CGIP* **13:** 279-297 (1980).
13. R. Nevatia, A color edge detector and its use in scene segmentation, *IEEET- SMC* **7(11):** 820-826 (1977).
14. R. B. Ohlander, Analysis of Natural Scenes, Ph.D. thesis, Carnegie-Mellon Univ., 1975.
15. Y. Ohta, et al., Color information for region segmentation, *CGIP* **13:** 222- 241 (1980).
16. F. Bumbaca, et al., Design and implementation of colour vision model for computer vision applications, *CVGIP* **39:** 226-245 (1987).
17. G. B. Coleman, Image Segmentation by Clustering, Ph.D. thesis, Univ. of Southern California, 1977.
18. A. L. Robertson, The CIE 1976 color difference formulae, *Color Research and Application* **2(1):** 7-11 (1977).
19. G. Wyszecki, et al., Color Science, Wiley, 1967.
20. R. H. Wallis, Film Recording of Digital Color Images, Ph.D. thesis, Univ. of Southern California, 1975.
21. W. T. Wintringham, Color television and colorimetry, *Proc. IRE* **39:** 1135-1172 (1951).
22. K. McLaren, The development of the CIE (L*, a*, b*) – uniform color space, *JSDC*, 338-341 (1976).
23. R. O. Duda, et al., Pattern Classification and Scene Analysis, Wiley, 1973.
24. N. Ahuja, et al., Neighbor gray levels as features in pixel classification, *PR* **12**, 251-260 (1980).
25. C. H. Chen, On the statistical image segmentation techniques, *Proc. IEEE Conf. Pat. Rec. and Image Proc.*, 1981, 262-266.
26. M. Celenk, et al., Gross segmentation of color images of natural scenes for computer vision systems, *Proc. SPIE* Vol. **635**, 1986, 333-344.
27. M. Celenk, Parametric-Histogramming Technique for Gross Segmentation of Color Images of Natural Scenes, Ph.D. thesis, Stevens Institute of Tech., 1983.
28. M. Celenk, et al., Color image segmentation by clustering and parametric histogramming technique, *Proc. Eight Int. Conf. Pat. Rec.*, 1986, 883-886.
29. M. Celenk, Modular design of the segmentation unit of hierarchical computer vision systems, *Proc. IEEE Int. Conf. Rob. and Aut.*, 1987, 372-379.
30. M. Celenk, An adaptive machine learning algorithm for color image analysis and processing, Proc. Int. Conf. Manufac. Science and Tech. of the Future, Cambridge, 1987.
31. M. Celenk, A parametric training algorithm for image understanding systems, *Proc. SPIE* Vol. **786**, 1987, 169-175.
32. S. Tominaga, Color image segmentation using three percep tual attributes, *Proc. Conf. Comp. Vis. and Pat. Rec.*, 1986, 628-630.
33. G. J. Klinker, et al., Image segmentation and reflection analysis through color, *Proc. SPIE* Vol.**937**, 1988, 229-244.
34. M. Celenk, An adaptive machine learning algorithm for color image analysis and processing, *Int. J. Rob. & Comp. Integ. Manufac.* **4(3/4):** 403-412 (1988).
35. M. Celenk, A color clustering technique for image segmentation, *CVGIP* **52:** 145-170 (1990).
36. M. Celenk, Colour image segmentation by clustering, *IEE Proc.-E* **138(5):** 368-376 (1991).

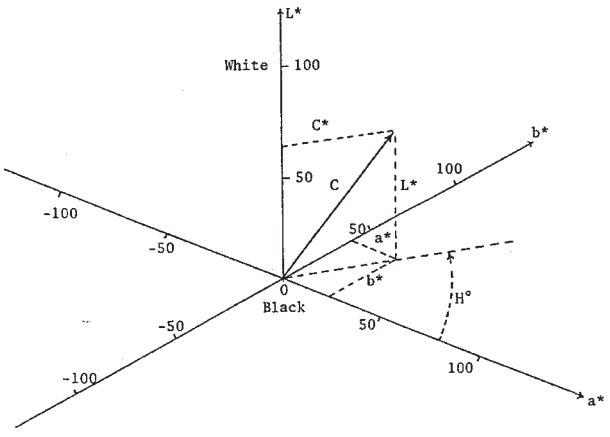

Figure 1. Organization of the (L, a*, b*) uniform color coordinate system.*

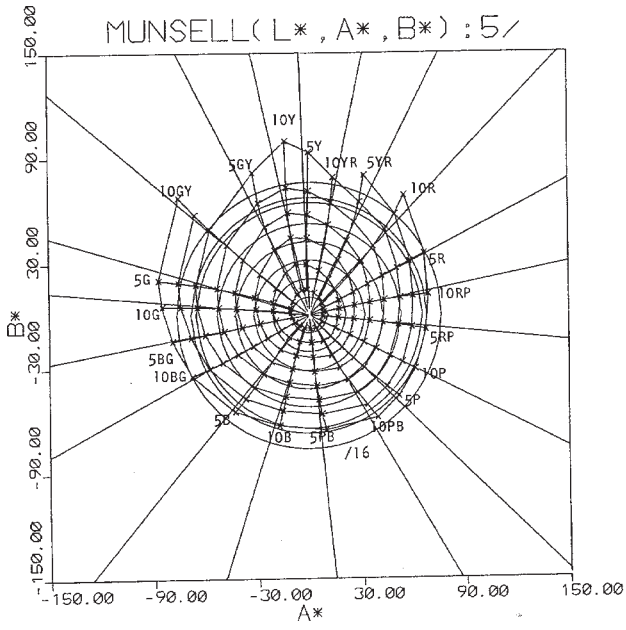

Figure 2. The loci of constant hue and constant chroma of Munsell system and their approximated networks (radial lines and concentric circles) in the (a, b*) plane at Munsell value of 5/.*

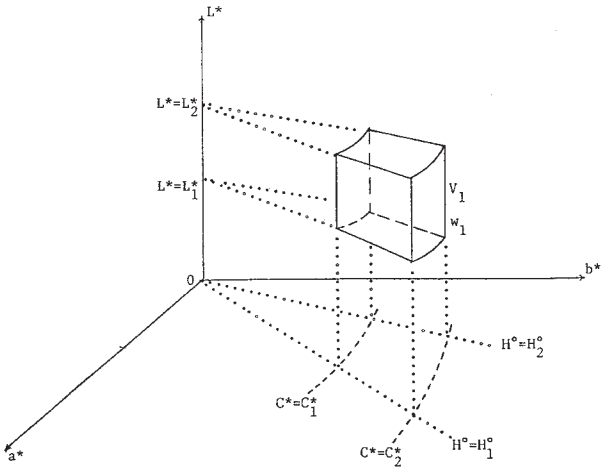

Figure 3. A circular-cylindrical decision element V_1 enclosing an image cluster w_1 in the (L, a*, b*) color space.*

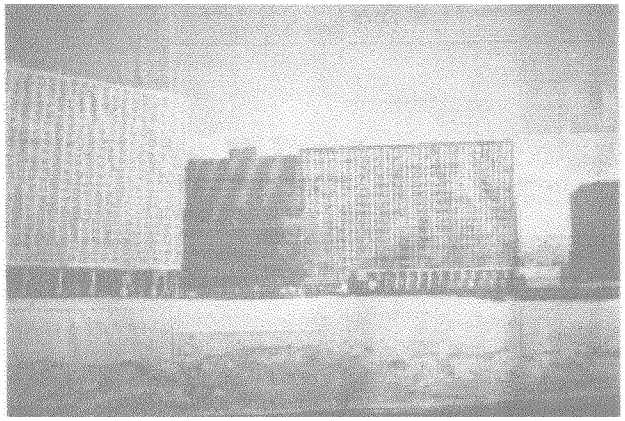

Figure 4. Photograph of the computer print out (using 32 gray levels) of the intensity value of the test image (picture "11").

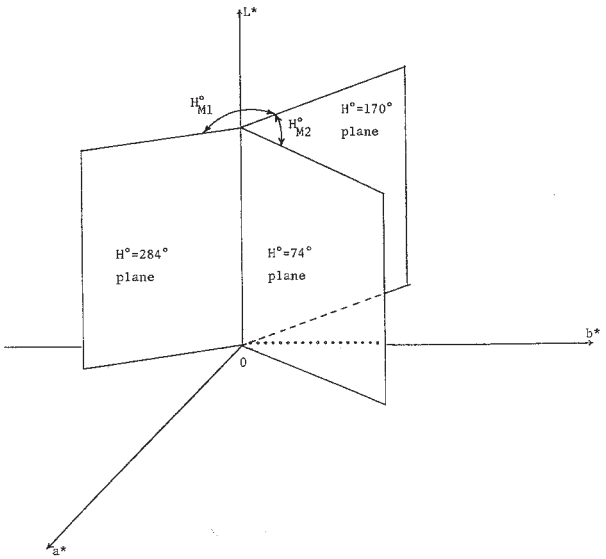

Figure 6. Angular hue planes describing the hue ranges of the best cluster (w_1) and its spectral neighbor (w_2) detected for the test image.

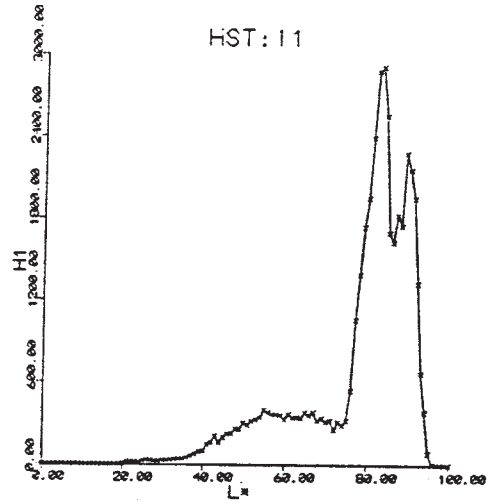

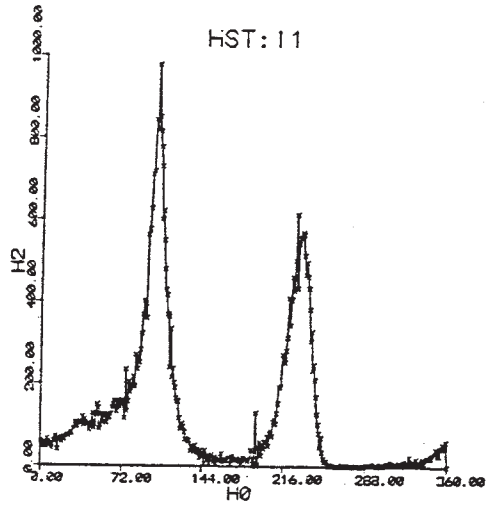

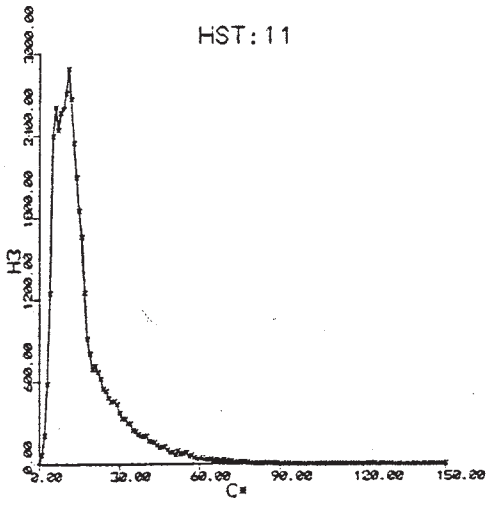

Figure 5. 1-D histograms of the L, H°, and C* cylindrical color components of the test image given in Fig. 4.*

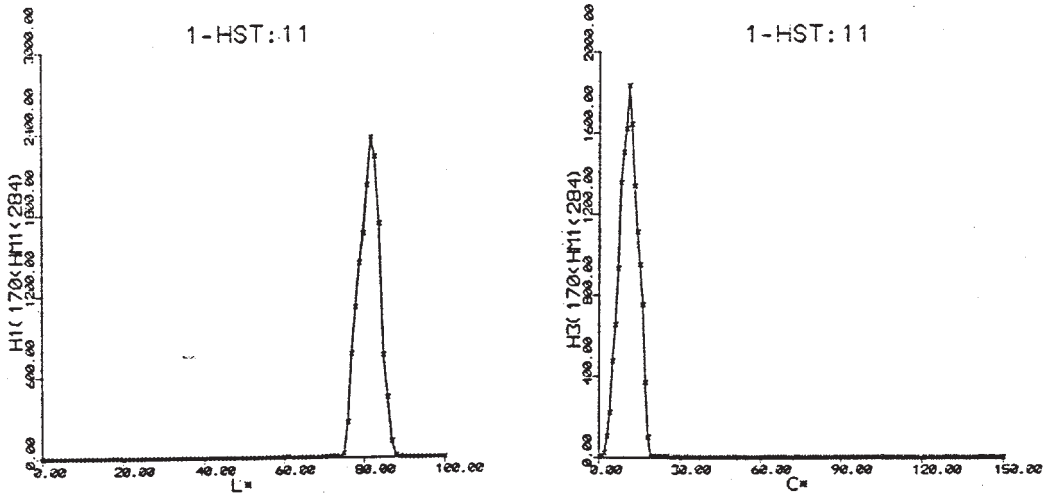

Figure 7. 1-D parametric histograms of the L and C* color components of the test picture constructed for mode 1.*

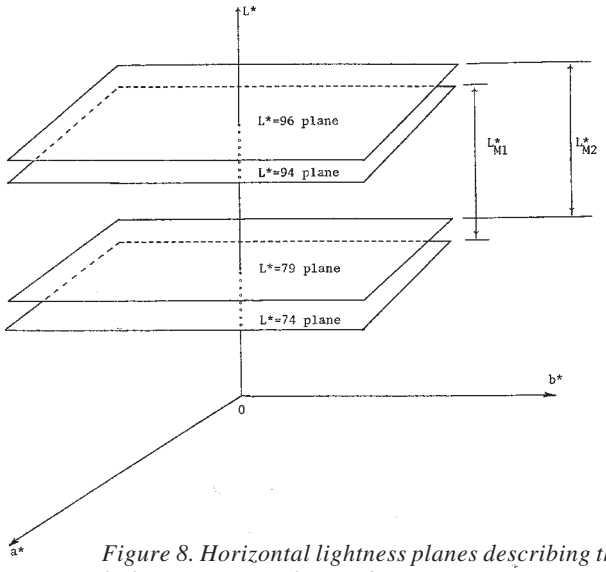

Figure 8. Horizontal lightness planes describing the lightness ranges of w_1 and w_2.

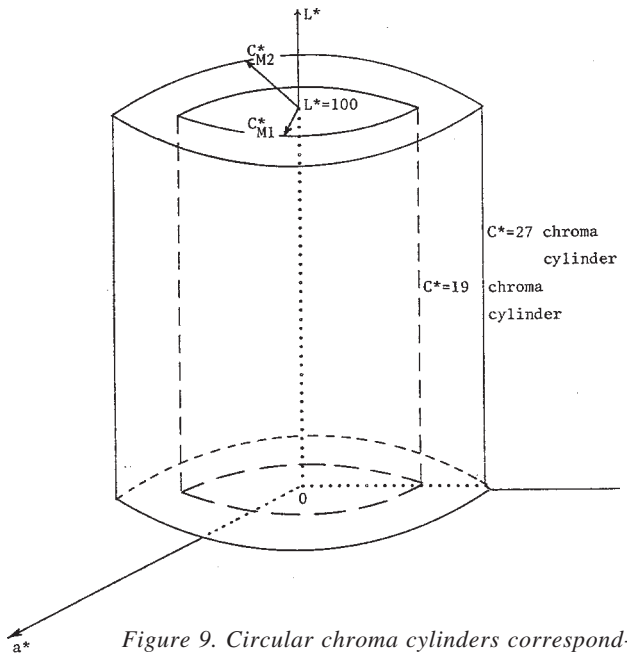

Figure 9. Circular chroma cylinders corresponding to the chroma ranges of w_1 and w_2.

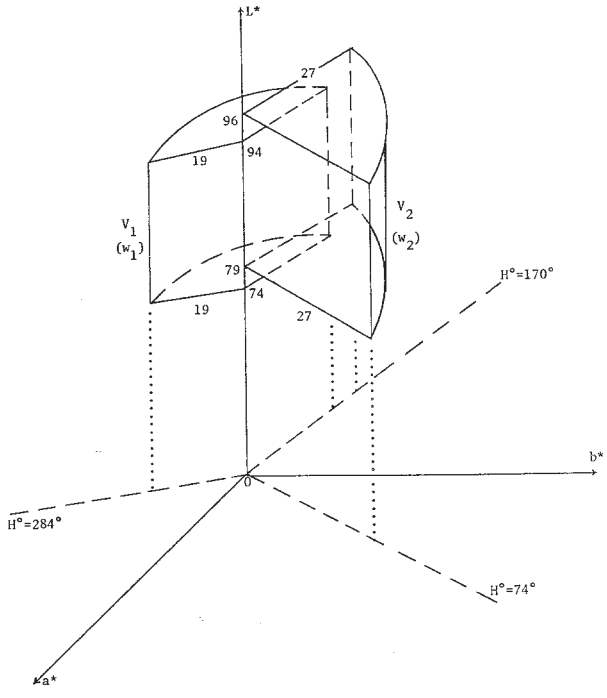

Figure 10. The estimated color distributions (V_1 and V_2) of w_1 and w_2 in the (L, a*, b*) space.*

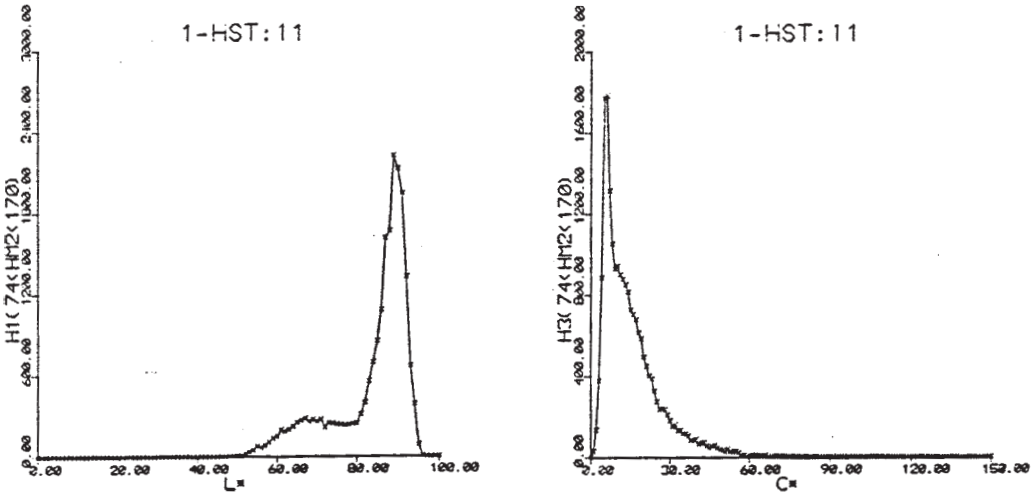

Figure 11. 1-D parametric histograms of the L and C* color coordinates of the test image derived for mode 2.*

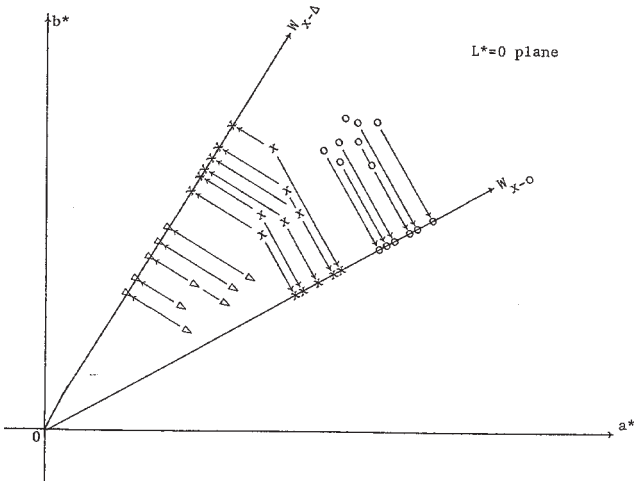

Figure 12. Two-at-a-time class projection process for separating the class "x" from its neighbors "o" and "Δ" in the (a, b*) plane.*

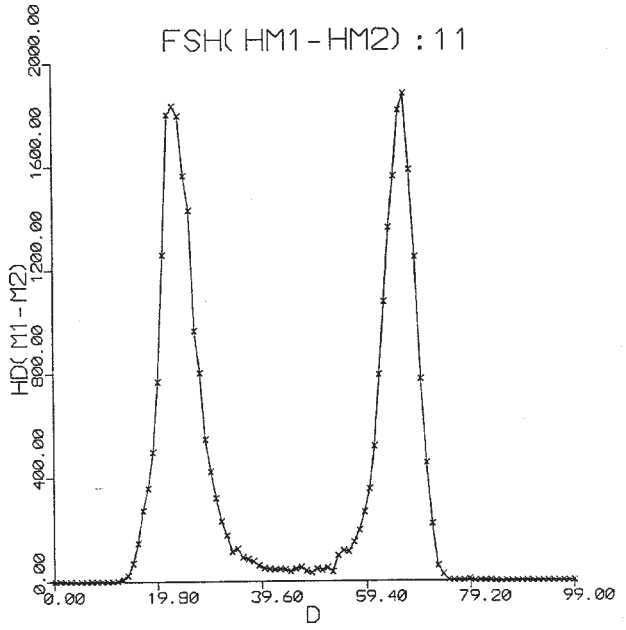

Figure 13. 1-D histogram of the projected values of color vectors belonging to w_1 and w_2, detected for extracting the image region "11:SKY".

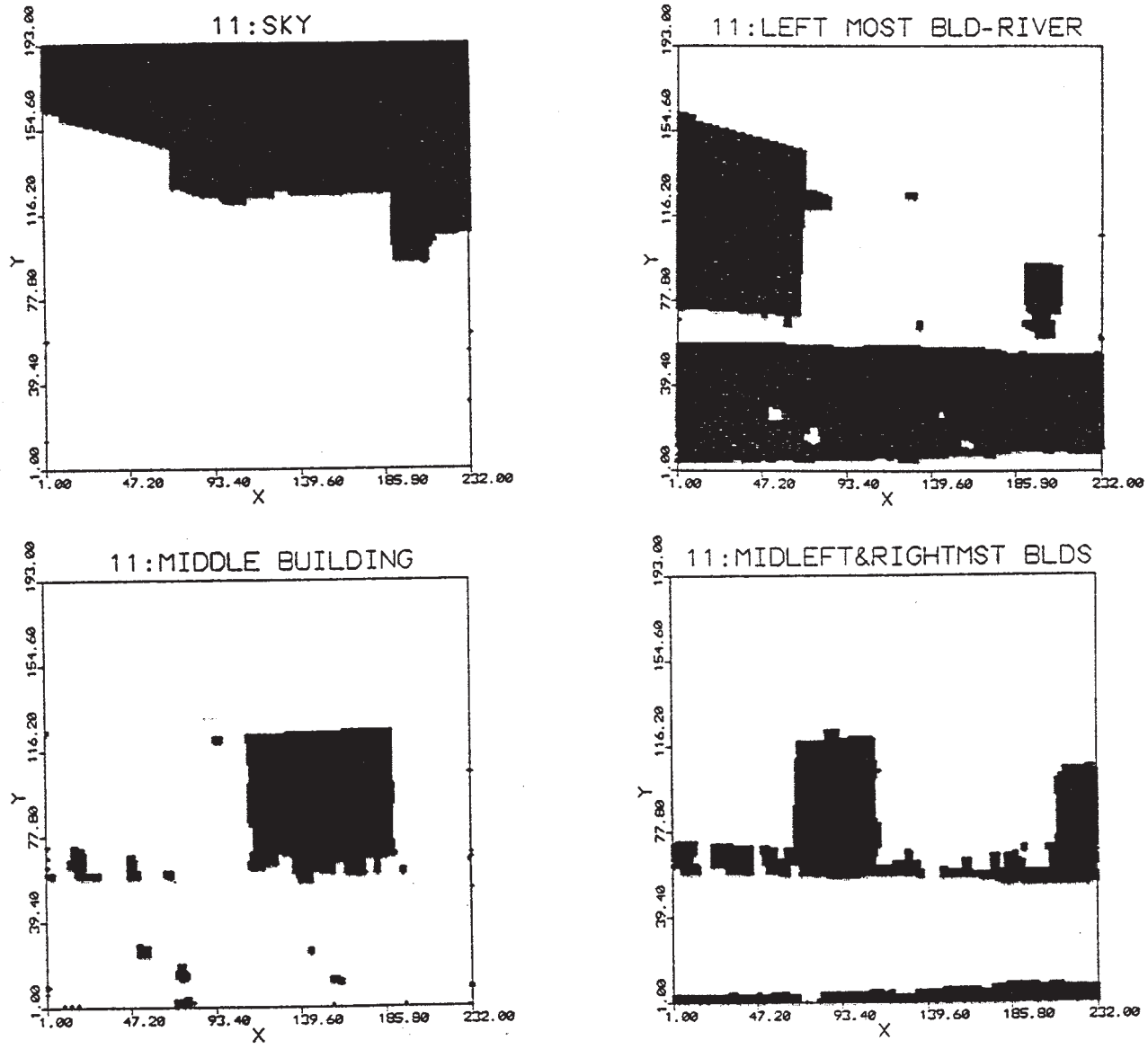

Figure 14. Image regions resulting from the segmentation of the test image (picture "11"). a) Image region "11:SKY" (top left). b) Image region "11:BLRI" (left most building and river) extracted by discarding the points of the detected region "11:SKY"(top right). c) Image region "11:APM"(midright building) extracted by excluding the pixels of regions in a and b (bottom left). d) Image region "11:APS"(midleft and rightmost buildings) detected by discarding the points of regions in a, b, and c (bottom right).

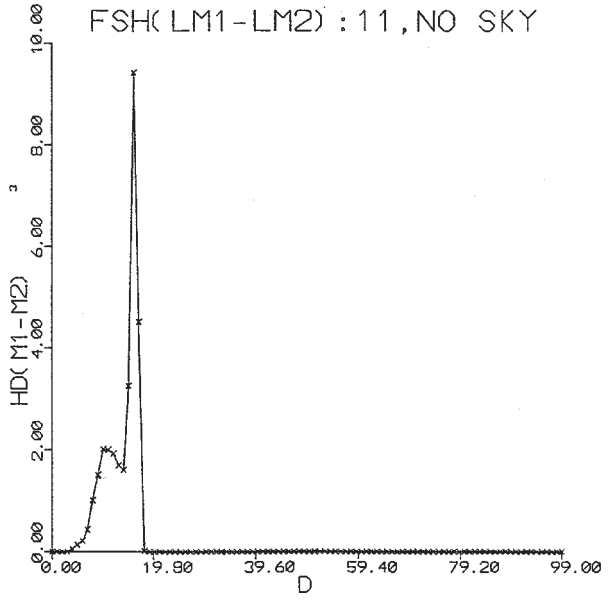

Figure 16. 1-D histogram of the projected values of color vectors belonging to the best mode and its neighbor, detected for extracting the image region "11:BLRI".

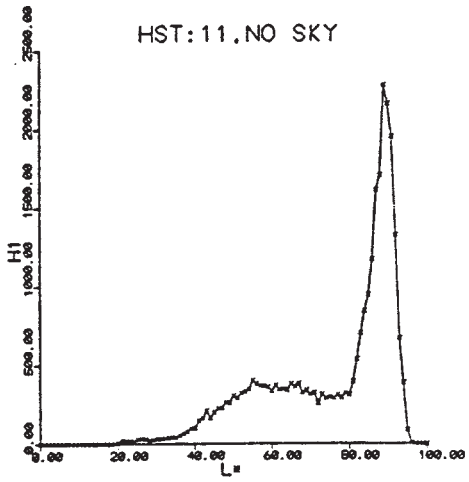

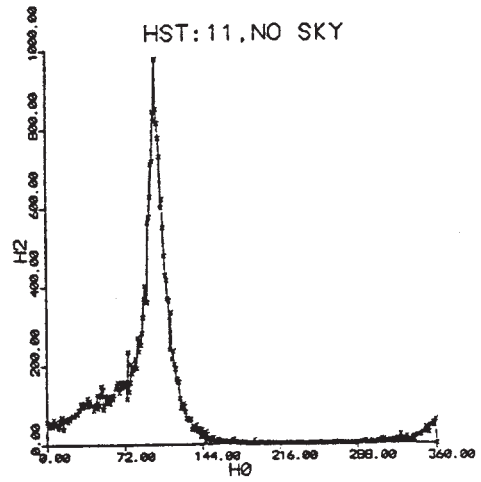

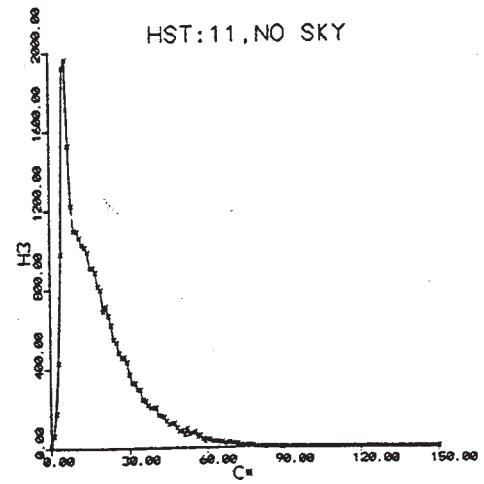

Figure 15. 1-D histograms of the L, H°, and C* color coordinates of the test image, constructed by excluding the points belonging to the sky.*

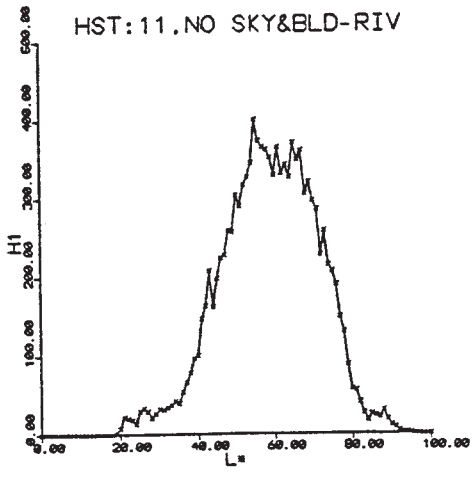

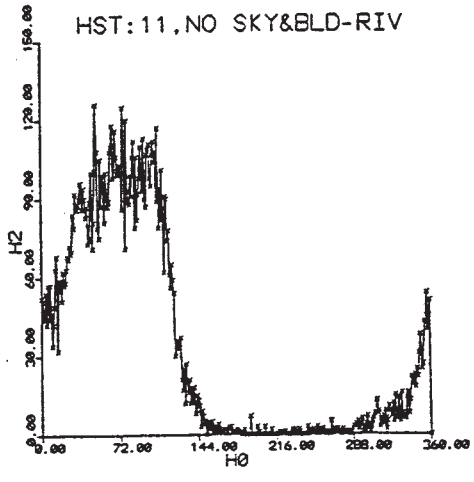

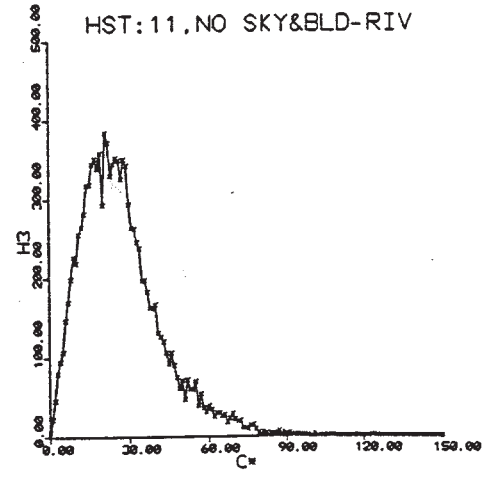

Figure 17. 1-D histograms of the L, H°, and C* color components of the test image, derived by discarding the points of the detected regions "11:SKY" and "11:BLRI"*

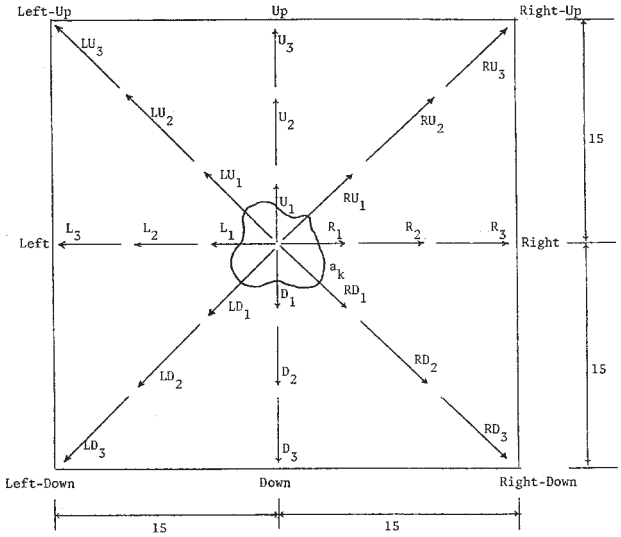

Figure 18. Eight fixed directions defined in the 30×30 *local window located at the center of gravity of an atomic region* a_k.

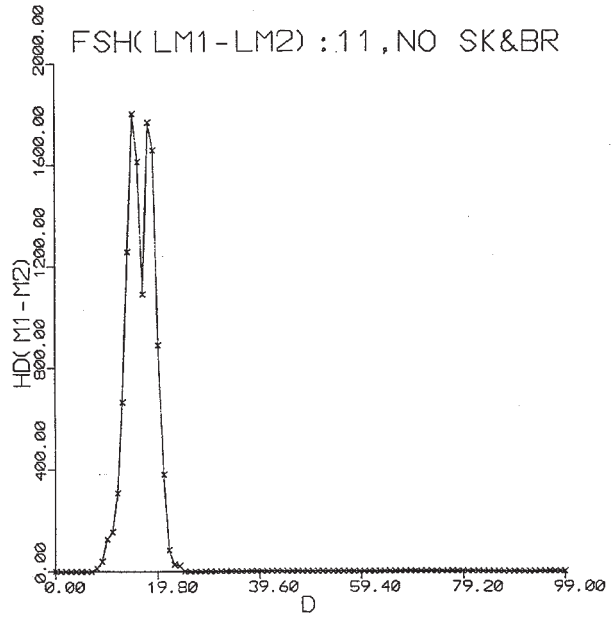

Figure 20. 1-D histogram of the projected values of feature vectors belonging to the modes detected for extracting the region "11:APM".

Figure 21. Photograph of the computer print out (using 32 gray levels on a logarithmic scale) of the intensity value of picture "9"

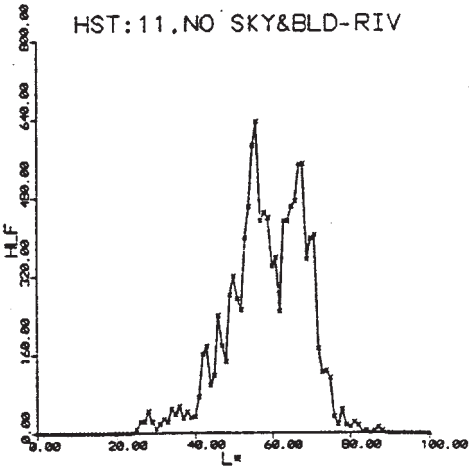

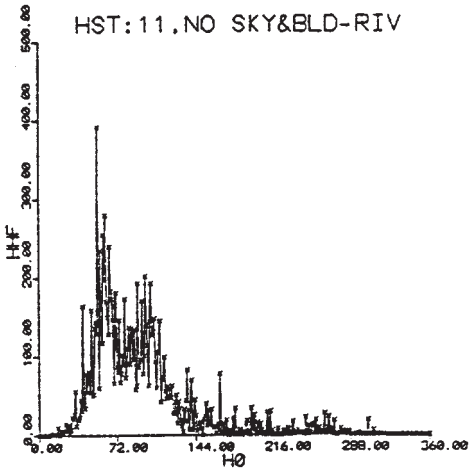

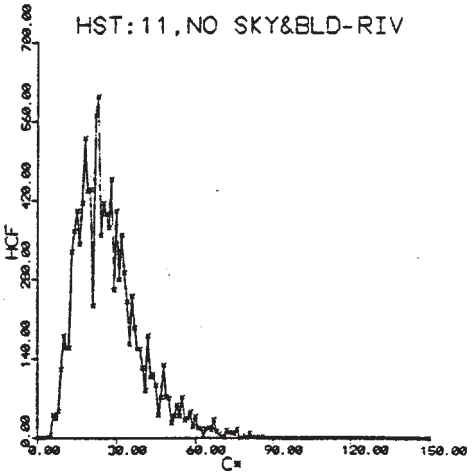

Figure 19. 1-D histograms of the L, H°, and C* components of the feature vector f, extracted for the remaining points of the test image.*

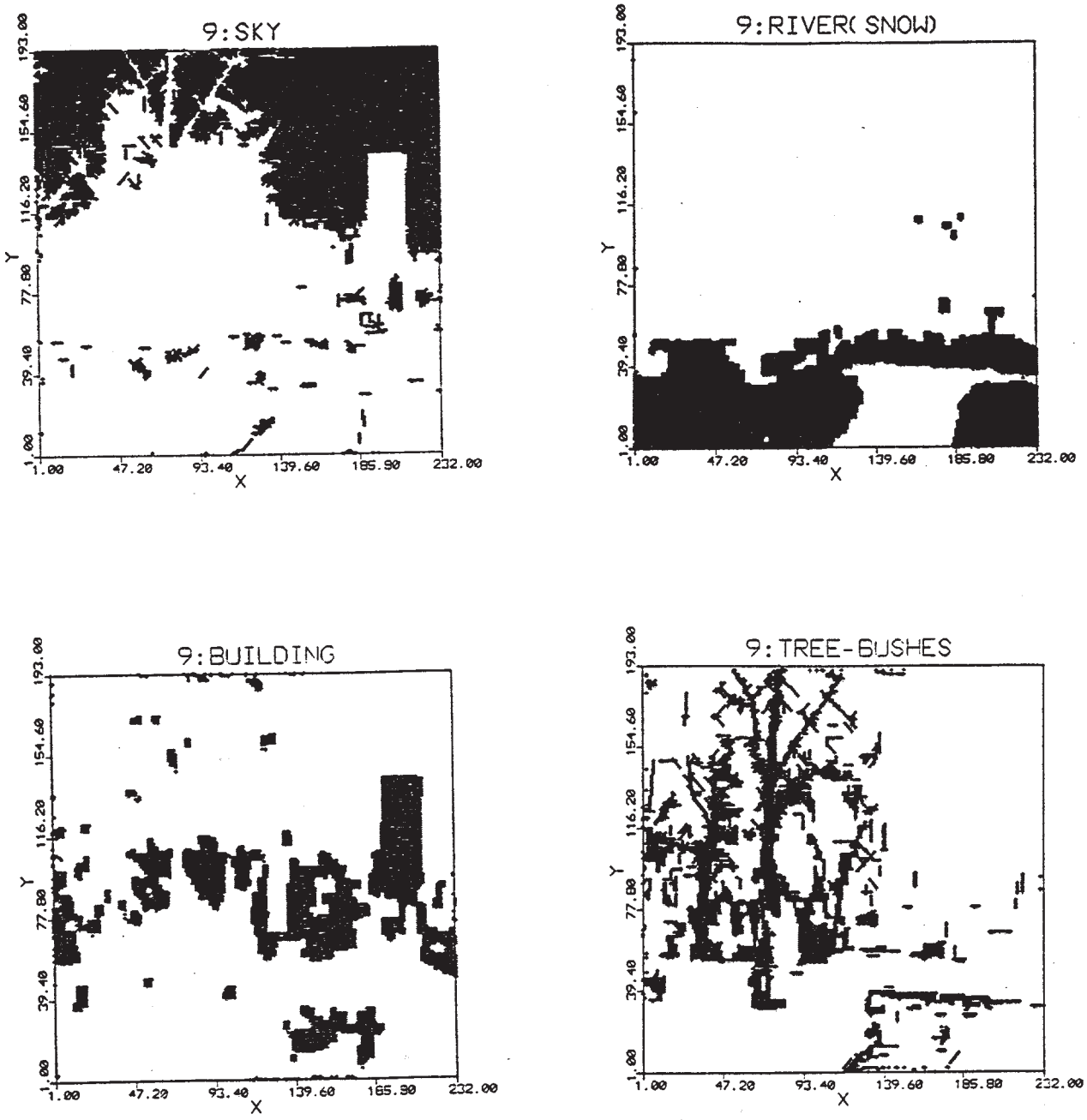

Figure 22. Segmentation results of picture "9". a) Image region "9:SKY" extracted for the sky (top right). b) Image region "9:RIV" corresponding to the river or snow (top left). c) Image region "9:BL" representing the building block (bottom left). d) Image region "9:TRE"obtained for the tree and bushes (bottom right).